GPS as a Solar observational instrument: Real-time estimation of EUV photons flux rate during strong, medium and weak Solar flares

Talwinder Singh,[1] M. Hernandez-Pajares,[2] Enric Monte,[3] A. Garcia-Rigo,[2] G. Olivares-Pulido[2]

[1]Department of Physics, Indian Institute of Technology (BHU) ,Varanasi, India.

[2]Departament Matem tica Aplicada IV, IonSAT res. group, Universitat Politcnica de Catalunya, Barcelona, Spain.

[3]Departament de Teoria del Senyal i Comunicacions, TALP res. group, Universitat Politcnica de Catalunya, Barcelona, Spain.

Abstract. In this manuscript, the authors show how the Global Navigation Satellite Systems, GNSS (exemplified in the Global Positioning System, GPS), can be efficiently used for a very different purpose from that for which it was designed; as an accurate Solar observational tool, already operational from the open global GPS measurements available in real-time, and with some advantages regarding dedicated instruments onboard spacecraft. The very high correlation of the solar Extreme Ultraviolet (EUV) photon flux rate in the 26-34 mm spectral band, obtained from the SEM instrument onboard the SOHO spacecraft during Solar flares, is shown with the GNSS Solar Flare Activity Indicator (GSFLAI). The GSFLAI is defined as the gradient of the ionospheric vertical total electron content (VTEC) rate versus the cosine of the Solar zenith angle in the day hemisphere (which filters out non-Solar over-ionization), and it is measured from data collected by a global network of dual frequency GPS receivers (giving in this way continuous coverage). GSFLAI for 60 X class flares, 320 M class flares and 300 C class flares, occurred since 2001, were directly compared with the EUV Solar flux rate data to show existing correlations. It was found that the GSFLAI and EUV flux rate present the same linear relationship for all classes of flares, not only the strong and medium intensity ones, X and M-class, as in previous works, but also for the weakest C-class Solar flares, which is a remarkable result.

1. Introduction

The scope of space geodesy technique applications is in continuous growth, in particular for measuring, in different and better ways, parameters of the Sun (see for instance *Soja et al.* [2014]). This is the context of the research and the results presented in this paper; the utilization of the Global Navigation Satellite Systems as an instrument of Solar observation by indirectly measuring the Solar EUV flux rate from the sudden over-ionization of the overall Earth ionosphere during Solar Flares.

Indeed, Solar flares are sudden flashes of brightness in the Solar atmosphere associated to energetic charged particle emission (primarily high energy protons) and electromagnetic (EM) radiation emission across the whole electromagnetic spectrum (primarily X rays and EUV rays). Solar flares generally originate in active regions, expanses of intense Solar magnetic field, and are often accompanied by coronal mass ejections (CMEs, see *Yashiro and Gopalswamy* [2008]). X-rays and EUV rays emitted during Solar flares can affect the Earth's ionosphere by producing photo electrons. These photo electrons are only produced in the daylight ionosphere and their enhancement can be approximated by the Chapman model (see *Mendillo et al.* [1974]). This enhancement in electron number results in increased reflection, refraction and diffraction of EM waves passing through the ionosphere, and hence can affect satellite communications. Solar flares also have an indirect adverse effect on the lifetime of satellites in the Earth's orbit. X-rays, along with EUV radiation, heat up the earth's outer atmosphere, causing it to expand. This, in turn, increases the drag acting on these Earth orbiting satellites, thus reducing their lifetime in orbit. Since EUV bands are optically thick in the Solar atmosphere, flares originating closer to the center of the Solar disk are more geo-effective than those closer to the limb (*Qian et al.* [2010]). Sometimes, after the arrival of a Solar flare radiation, associated nearly-relativistic electrons can also arrive, typically several minutes after the onset of the EM signature of the Solar flare (*Simnett et al.* [1974] and Fig. 6 in *Hernández-Pajares et al.* [2012]), which may affect the readings of direct sensors such as the SOHO SEM. But since these electrons enter the Earth's atmosphere through the polar caps, the associated increase in ionization in the atmosphere does not follow the expected flare overionization dependence of the Solar zenith angle, and then it can be filtered-out.

Dual Frequency GPS satellites have become an excellent tool for ionosphere monitoring today. The total number of permanent GPS receivers around the globe, whose data is provided by the International GNSS Service (IGS, see *Dow et al.* [2009]), is currently more than 300, giving high spatial and temporal resolution to measure the electron content in the ionosphere. In the following sections we will show how Solar flares can be monitored using GPS data and how the high geo-effectiveness of Solar EUV radiation allows for the determination of its flux rate by measuring the ionospheric response to Solar flares. A previous study by *Hernández-Pajares et al.* [2012] on this subject mainly focused, and demonstrated the approach, for X class flares. Recently, this GNSS-ionospheric proxy of the Solar EUV flux rate has been used to characterize the main statistical properties of Solar flares (*Monte-Moreno and Hernández-Pajares* [2014]). The present paper covers M and C class flares along with X class flares, showing that the same approach is also valid for mid and low intensity Solar flares.

The organization of the manuscript is as follows: Section 2 explains the GSFLAI, an approach introduced in *Hernández-Pajares et al.* [2012] to detect and characterize Solar flares. Section 3 explains how dual frequency GPS data can be used to calculate total electron content. In sections 4 and 5, information regarding input GPS data and reference EUV data is given. Section 6 discusses Solar flare events and results. This paper is concluded in Section 7.

2. The GNSS Solar flare activity indicator (GSFLAI)

During a Solar flare event, the ionospheric electron density increases very rapidly. Therefore the assumption that the change in electron density is only due to the ionization process and not resulting from loss due to recombination processes or physical migration is valid. Indeed, it can be seen that the rate of production of ion-electron pairs at some level of the atmosphere (typically in equilibrium at any given time with the losses by recombination) is proportional at any given time to the intensity of the ionizing radiation (see for instance Eq. 1.19 in page 15 of *Hunsucker & Hargreaves* [2002]). It is then straightforward to derive that, under a sudden increase of Solar radiation (where transport phenomena can typically be neglected), an increase in the rate of production of ion-electron pairs will occur, with the associated sudden generation of extra free electrons. This is exactly what is observed for the main Solar flares (in *Hernández-Pajares et al.* [2012]), and for low intensity flares (as we are going to show in this manuscript). Then the rate of VTEC $\dot{V}$, for a given Solar zenith angle χ, is related to the Solar flux rate $\dot{I}$ by the following equation:

$$\dot{V} = \eta' \cdot C(\chi) \cdot \dot{I} \tag{1}$$

where η' stands for geo-effectiveness of the considered spectral range.

It has been shown that $C(\chi)$ can be reasonably approximated by $\cos\chi$ for all values of χ

(Hernandez-Pajares et al. 2012). Since the ionization process takes place a few hundred kilometers above Earth's surface, enhanced ionization for $\chi > 90$ degrees can be expected due to the Solar irradiance at such height. On plotting $\dot{V}$ against $\cos\chi$ for different Solar flare events, enhanced ionization is clearly visible for $\cos\chi > -0.2$. Thus when $\dot{V}$ is plotted against $\cos\chi$ for $\cos\chi = -0.2$ to 1, a straight line is observed described by the equation:

$$\dot{V} = a_1 \cos\chi + a_2 \tag{2}$$

The independent term, a_2, is expected due to enhanced ionization for $\chi > 90\,\mathrm{deg}$. In this paper, GSFLAI is considered as the slope of this line, i.e. a_1, and it is adjusted as a single parameter to enhance the estimation (assuming over-ionization for $\cos\chi > -0.2$, corresponding approximately to the ionospheric effective height). From Eq. 1 and 2, it is clear that with this definition, the GSFLAI is linearly related to the Solar flux rate $\dot{I}$ with a certain slope and an intercept whose magnitude is directly related to the over-ionization at $\cos\chi = 0$, i.e. a_2.

3. VTEC from GPS data

TEC is the total number of electrons between two points along a cylinder of cross-section one meter squared. Slant TEC(STEC) can be defined as the total number of electrons between a satellite and a receiver along a 1 m^2 cylinder, i.e. the corresponding integral of the electron density N_e:

$$S = \int_{r_r}^{r_s} N_e \cdot dl \tag{3}$$

where r_s and r_r represent the transmitting satellite and receiver positions, respectively. Vertical TEC (VTEC) then corresponds to the STEC when the satellite-zenith angle is zero.

Ionospheric observations are generally derived from dual-frequency GPS phase measurements (L_1 and L_2) in terms of the "Ionospheric combination of carrier phases" L_I. It provides a direct but ambiguous measurement of STEC, S, with a nominal error of 0.02 TECU, where 1 $TECU = 10^{16} m^{-2}$ (see for instance *Hernández-Pajares et al.* [2011]). L_I can be expressed in terms of S as:

$$L_I \equiv L_1 - L_2 = \alpha.S + w_I + B_I \tag{4}$$

where $\alpha = 1.05 \times 10^{-17}\ m^3$, w_I is due to the wind up effect which is easily corrected for permanent stations and B_I is the ambiguity term, which cancels out when considering the rate of L_I (taking into account the fact that no cycle slips have occurred).

Vertical TEC is estimated from STEC by assuming a simple 2D ionospheric model i.e. the ionospheric electron content is considered to be situated at 450 km above the Earth´s surface. Nevertheless, this is not a relevant parameter in this problem due to the predominant data available at high elevations (where the assumed mapping is very accurate), the elevation mask used (15 degrees) and the overall fitting and outlier removal processes (performed at every epoch) versus the cosine of the Solar-zenith angle for filtering out of extreme cases. The VTEC rate can be written as

$$\dot{V} \equiv \frac{\partial V}{\partial t} \simeq \frac{1}{M}\frac{\Delta S}{\Delta t} = \frac{1}{\alpha M}\frac{\Delta L_I}{\Delta t} \tag{5}$$

where $M \simeq \frac{1}{\cos Z}$ is called the ionospheric mapping function, which is the de-projection coefficient from the vertical to line-of-sight (slant) directions calculated from the satellite zenith angle Z (the detailed expression can be found as well in *Hernández-Pajares et al.* [2011]).

Therefore, from Eq. 2 and 5 taking into account Eq. 1, our targeted magnitude for, the Solar flux rate $\dot{I}$, can be computed.

4. Input Data

The input global GPS data are acquired from the IGS association, a voluntary federation that provides open access to high quality GNSS data and products. It provides data from more than 300 dual frequency GPS receivers distributed worldwide and which are capable of ionospheric monitoring with high spatial resolution (see *Hernández-Pajares et al.* [2009]). The time series of GNSS measurements captured at a sampling period of 30 seconds were used in this paper. These time series are available at `ftp://cddis.gsfc.nasa.gov/gps/data/daily/`. In general, 4 to 8 values of STEC can be computed from a single receiver, corresponding to different line of sight directions for several GPS satellites in view, covering in this way most of the values of Solar zenith angle χ. Presently, it is running in real-time, with a latency of 30 seconds, and since 2012 has been used in the context of the ESA MONITOR and MONITOR-2 projects (see *Beniguel et al.* [2012] and *Hernández-Pajares et al.* [2015] respectively), supported also by the RTIGS project (see *Caissy et al.* [2012]).

5. Reference Data

GSFLAI calculations obtained from global GPS network data were compared with EUV measurements taken done by **S**olar **E**UV **M**onitor (SEM) on-board **So**lar and **H**eliospheric **O**bservatory (SOHO, see *Judge et al.* [1998]) to obtain a relation between GSFLAI and EUV flux rate. EUV Solar flux data provided in the range 26-34 nm were used in this study. This choice was motivated by the fact that this range is dominant in the total

EM emissions by active regions, and also the high absorption of this range at Earth's ionosphere, mostly by atomic oxygen (dominant species and source of ionization up to 500 km). Also, the classification of Solar flares into X, M and C class flares was performed based on the X-Ray intensity data provided by the **X**-**R**ay **S**ensor (XRS) instrument on-board **G**eosynchronous **O**perational **E**nvironmental **S**atellite (GOES, *Garcia* [1994]).

6. Solar Flare Events and Results

To study the validity of GSFLAI as a potential Solar flare detector (complementing the Sunlit Ionospheric Sudden TEC Enhancement Detector, SISTED; see *García-Rigo* [2012]) and a proxy for the EUV flux rate, 60 X class flares, 320 M class flare and 300 C class flares that occurred between January 2001 and March 2014 were chosen. These flares were selected from the pool of total flares which were clearly picked-up by the SEM sensor on-board SOHO:

1. GSFLAI was computed for all the X and M class flares from Jan 2001 to March 2014. Because a large number of C class flares occurred during this period, we only considered C class flares that occurred on same days as X or M class flares. This prevented us from downloading any extra data while maintaining the sample unbiased.

2. Some of these flares were not picked up by the SEM, most probably because they originated close to the Solar limb (but they were picked up by the GOES X-Ray sensor as the X-Ray band is transparent in the Solar atmosphere). Because of the large number of total flares in our sample, we devised an automatic method to reject those flares from the study which were not picked up by the SEM. The method was to compare the epochs at which the GSFLAI and EUV flux rate achieved their maximas after the onset of the

flare. If both epochs were within 50 seconds of each other, then the flare concerned was considered fit for study.

Section 6.1 discusses the validity of the GSFLAI method for the detection of various intensities of Solar flares. Also, the correlation of the GSFLAI with the EUV flux rate is shown for representative flares of different intensities. In section 6.2, the GSFLAI is directly compared with the EUV flux rate for all the Solar flares studied in this paper, to show that a linear relationship exists between the GSFLAI and EUV flux rate and to compute their linear relationship equation.

6.1. Representative GSFLAI examples

To demonstrate how the GSFLAI is computed during a Solar flare and to aid visualization, one plot for each Solar flare intensity class (X, M and C) are shown in Fig. 1. Some outliers have been removed from the data, mainly due to local ionospheric perturbations and carrier phase measurement errors which do not follow the expected dependence with Solar zenith angle. It is clearly visible that the rate of change of VTEC ($\dot{V}$) shows a linear relation to $\cos\chi$, where $\cos\chi$ ranges from -0.2 *to* 1.0. After removing the outliers by rejecting the points having an error greater than twice the standard deviation, in a first least squares linear fitting, a final straight line is fitted through the data at each epoch (e.g. each 30 seconds, or each second). The GSFLAI is defined as the slope of this line. It is clear from the figure that the ionization effect is maximum for X class flares, followed by M and C class flares, respectively. But it will be later shown that this might not always be the case. Also, as mentioned earlier, the occasional nearly-relativistic electrons associated with certain Solar flares enter the Earth's atmosphere through the polar caps. Since the increase in atmospheric ionization due to these electrons is not a function of the Solar zenith angle, the GSFLAI is not affected by them (*Hernández-Pajares et al.* [2012]). Also, the time evolution of the GSFLAI and EUV flux rate will be shown together to demonstrate the correlation between the two types of data. The top panel of Fig. 2 shows the time evolution of the GSFLAI and the EUV flux rate for an X class Solar flare classified as X6.2 according to GOES X-Ray flux data. It can be seen that they are well correlated. There are two points to note here:

1. The EUV measurements by SEM-SOHO are lagging behind the GSFLAI measurements by 20-30 seconds. This lag, which is corrected for, is coincident with the one found by *Hernández-Pajares et al.* [2012] working at 1 Hz, and it is smaller than the time resolution of the GPS data used in this study (30 seconds).

2. After a peak in the GSFLAI and EUV flux rate, the GSFLAI is not able to follow the EUV rate (GSFLAI decreases slowly), likely due to the slow recombination rate of the ionosphere compared to its sudden ionization rate.

Furthermore, the typical correlation between GSFLAI and EUV flux rate is shown for M and C class flares in the middle and bottom panels of Fig. 2, respectively. An M3.5 flare that occurred on 30 November 2001 and a C5.3 flare that occurred on July 22 2004 are chosen for this. A very good correlation can be seen in both cases. An important thing to observe is that the GSFLAI (and EUV flux rate) presents a higher peak in the case of the (weeker) C5.3 flare. This result stems from the fact that flare classification is made on the basis of the X-Ray flux, which is relatively transparent to the Solar atmosphere, in contrast to the EUV rays. Therefore a lot of EUV radiation is absorbed in the Solar atmosphere if the source of the Solar flare is farther from the Solar disk center. This is true in this case as the source of the C5.3 flare was located closer to the Solar disk center (N04E10) when compared to the source of the M3.5 flare (S07E54). Indeed, the location of the flare in the Solar disc is important for the ionospheric response to the flare. The influence of the flare's location has already been studied and discussed in *Hernández-Pajares et al.* [2012] in which the excellent correlation between the direct EUV Solar flux rate and ionospheric over-ionization (measured at a global scale by many GPS receivers) was not observed when the X-band Solar flux rate was considered. In this way, by considering a simple model (dependence on the cosine of the Solar flare angular distance to the Solar disc center) for the EUV flux extinction in the Solar atmosphere (which does not affect the X-band radiation, as it is well known), both kind of measurements were in agreement, as is shown in Fig. 9 of *Hernández-Pajares et al.* [2012].

Similar to the relationship between the GSFLAI and the SOHO-EUV flux rate, we find a good correlation between the GSFLAI and GOES-EUVI irradiance rate (see Fig. 3). At the moment, the GOES EUV irradiance data is only available at the cadence of 1 minute from `ftp://satdat.ngdc.noaa.gov/sem/goes/data/new_avg`. Future work can focus on extending the study of the relationship between GSFLAI and the GOES-EUVI irradiance rate.

Nevertheless, it can be seen that, in the case of low and mid geo-effectiveness Solar flares, the amount of noise could masks the shape of the underlying function between the cosine of χ and the GSFLAI index. Although the method used in this work allows for the rejection of the outliers, and therefore allows finding of the correct slope, which is consistent with the hypothesis of the model as shown in Eq. 1, it does not allow for the fact that there might be other dependencies that are not captured by the model. In particular, by trying another method (one-dimensional median filter -*Pratt* [1979]- plus a zero phase low pass filter designed by means of the Kaiser window -*Hamming* [1989]-) we have found that for weak and mid-intensity flares, the underlying dependency consistently manifests some consistent nonlinear dependencies (low-frequency oscillations along the regression line, see Fig. 4), which deserves investigation in further work.

6.2. Relationship between GSFLAI and direct EUV flux rate measurements

Direct comparison of the GSFLAI and the SOHO/SEM Solar EUV flux rate is shown in Fig. 5 for strong, mid and weak Solar flares. An almost linear relationship is observed, which is in full agreement with Eq. 1. Table 1 summarizes the linear relationships obtained on linear fitting of the data (fifth and seventh columns on one hand, and sixth and eigth columns on the other hand -filtered in the last case to points with maximum ionization increase per flare-). It was observed that the slope of these fittings (0.18, 0.13 and 0.11 TECU/10^9/cm^2/s for X, M and C class Solar flares with correlation factors 0.83, 0.63 and 0.46, respectively) are in agreement, but with some initial differences for each class. Indeed, the slope is slightly greater for strong Solar flares and slightly lower for weak Solar flares. This effect is attributed to two reasons:

1. Points considered immediately after a peak in GSFLAI are not so well correlated with the EUV flux rate, likely due to the slower recombination rate. This effect is predominant in higher intensity flares so that they show a slightly greater slope of GSFLAI vs EUV flux rate.

2. The measurement/modelling of noise in lower intensity flares tends to decrease the slope of the GSFLAI vs EUV flux rate graph.

To check the validity of the above explanations, we plotted only those points corresponding to the highest GSFLAI for each given flare and which had an EUV flux rate (in units $photons \cdot 10^9/cm^2/s^2$) greater than 0.0075[1]. Points satisfying this criteria are plotted in Fig. 6 along with their regression line. This resulted in the selection of only those points that corresponded to maximum ionization, rather than recombination and were less affected by measurement/modelling noise. Fitting a straight line to these points gave almost identical results (slopes of 0.152-0.159 TECU/10^9/cm^2/s) for all intensities of flare. These results are summarized in Table 1 (columns 4 and 6). We also observe in the same table, that the correlation factor of the GSFLAI vs EUV flux rate data increases very significantly after restricting our selection of data points as mentioned above (up to 0.94, 0.70 and 0.94 for X, M and C classes, respectively). This result confirms that other sources of ionospheric activity such as that of Medium Scale TIDs (see for example *Hernández-Pajares et al.* [2012b]), geomagnetic storms or scintillation, are mostly filtered out in our model. This is due to the fitting requirement at each epoch such that the VTEC rate measurements should be dependent on the Solar-zenith angle computed in the ionospheric pierce point (IPP) in the ionospheric thin shell, χ (see Eq. 2), either for the weakest C-class flares.

Also as explained in Section 2, we observe that, as expected, the *intercept* is greater for those flares that cause more ionization at $\cos\chi = 0$, which is generally in the decreasing order of X, M and C class flares.

7. Conclusions

Through this paper, it is demonstrated how GNSS (by means of the GNSS Solar Flare Activity Indicator, GSFLAI) can become an efficient Solar observational instrument in the characterization of all of kinds of geo-effective Solar flares with remarkable accuracy (which can be better than that of direct EUV flux detectors on board spacecraft[2]). Indeed, an extensive study of X, M and C class flares occurred between January 2001 and March 2014 confirmed the use of GSFLAI as a proxy for EUV flux rate direct measurements (taken from the SOHO Solar probe instrument) during such strong, mid and even weak Solar flares, in a very consistent way. Such confirmation has been extended by first time to a second Solar probe providing direct EUV measurements; the GOES-EUVI data. In this way, global real-time networks of GNSS receivers (such as the one supporting the above mentioned MONITOR project) are already becoming Solar sensors. This role extends the previous usage of GNSS data to detect and characterize Solar flares (an example is the Sunlit Ionosphere Sudden TEC Enhancement Detector, SISTED, see section 7.4 in *Hernández-Pajares et al.* [2012]).

Acknowledgments. The data for this paper are available and it can be requested to any of the authors, in particular to Talwinder Singh (talwinder.singh.app11@iitbhu.ac.in) and Manuel Hernández-Pajares (Manuel.Hernandez@upc.edu). The solar flare detection technique was developed in the context of the authors participation in the ESA MONITOR activity, under a contract of the European Space Agency in the frame of the European GNSS Evolutions Programme. This work has been partially supported by project TEC2012-38939-C03-02 funded by the Spanish Ministry of Science and Innovation.

Notes

1. These points are, for instance, suitable for defining a proxy of the geophysical intensity of the flare, once the effect of distance to the Solar disc center is corrected, as was shown in *Hernández-Pajares et al.* [2012] (Fig. 9 and associated comments).
2. Which can be affected, in particular, by huge measurement error sources such as the arrival of relativistic electrons, sometimes simultaneously emitted with the flare, which however do not affect the GNSS-based technique (see *Hernández-Pajares et al.* [2012], top plot of Fig. 6).

References

Beniguel, Y. et al. (2012, December). Ionospheric Effects on GNSS Performance. In Satellite Navigation Technologies and European Workshop on GNSS Signals and Signal Processing,(NAVITEC), 2012 6th ESA Workshop on (pp. 1-8). IEEE.

Caissy, M., L. Agrotis, G. Weber, M. Hernandez-Pajares and U. Hugentobler (2012), The International GNSS Real-Time Service, GPS World, June 2012.

Dow, J., R. Neilan, and C. Rizos (2009), The international GNSS ser- vice in a changing landscape of global navigation satellite systems, J. Geod., 83(34), 191198, doi:10.1007/s00190-008-0300-3.

Garcia, H. A. (1994), Temperature and emission measure from goes soft X-ray measurements, Sol. Phys., 154(2), 275308.

García-Rigo, A. (2012), Contributions to ionospheric determination with Global Positioning System: solar flare detection and prediction of global maps of Total Electron Content, Ph.D. dissertation. Doctoral Program in Aerospace Science and Technology, Universitat Politecnica de Catalunya, Barcelona, Spain.

Hamming, R.W. (1989), Digital filters, Prentice-Hall.

Hernández-Pajares, M., J. M. Juan, J. Sanz, A. García-Rigo, J. Feltens, A. Komjathy, S. C. Schaer, and A. Krankowski (2009), The IGS VTEC maps: A reliable source of ionospheric information since 1998, J. Geod., 83(34), 263275.

Hernández-Pajares, M., J.M. Juan, J. Sanz, A. Aragón-Àngel, A. García-Rigo, D. Salazar, M. Escudero (2011), The ionosphere: effects, GPS modeling and the benefits for space geodetic techniques, J. Geod., 85, 887907, doi:10.1007/s00190-011-0508-5.

Hernández-Pajares, M., A. García-Rigo, J. M. Juan, J. Sanz, E. Monte and A. Aragón-Àngel (2012), GNSS measurement of EUV photons flux rate during strong and mid solar flares, SPACE WEATHER, VOL. 10, S12001, doi:10.1029/2012SW000826.

HernándezPajares, M., Juan, J. M., Sanz, J., & AragónÀngel, A. (2012). Propagation of medium scale traveling ionospheric disturbances at different latitudes and solar cycle conditions. Radio Science, 47(6).

Hernández-Pajares, M., R. Prieto-Cerdeira, Y. Béniguel, A. García-Rigo, J. Kinrade, K. Kauristie, R. Orus-Perez, S. Schlueter, D. Serant, B. Nava, A. Krankowski, H. Secretan, R. Sampedro and X. Prats, MONITOR ionospheric monitoring system: analysis of perturbed days affecting SBAS performance, Proceedings of the ION 2015 Pacific PNT Meeting, Institute of Navigation, pages 970 - 978.

Hunsucker, R. D., & Hargreaves, J. K. (2002). The high-latitude ionosphere and its effects on radio propagation. Cambridge University Press.

Judge, D. L., et al. (1998), First solar EUV irradiances obtained from SOHO by the Celias/Sem, Sol. Phys., 177(12), 161173.

Mendillo, M., et al. (1974), Behavior of the ionospheric F region during the Great Solar Flare of August 7, 1972, J. Geophys. Res., 79(4), 665672.

Monte-Moreno, E., and M. Hernández-Pajares (2014), Occurrence of solar flares viewed with GPS: Statistics and fractal nature, J. Geophys. Res. Space Physics, 119, doi:10.1002/2014JA020206.

Pratt, W.K. (1978), Digital Image Processing, John Wiley & Sons, New York, vol. 1191, pp. 491-556.

Simnett, G. M. (1974), Relativistic electron events in interplanetary space, Space Sci. Rev., 16(1-2), 257323.

Soja, B., Heinkelmann, R., & Schuh, H. (2014). Probing the solar corona with very long baseline interferometry. Nature communications, 5.

Qian, L., A. G. Burns, P. C. Chamberlin, and S. C. Solomon (2010), Flare location on the solar disk: Modeling the thermosphere and ionosphere response, J. Geophys. Res., 115, A09311, doi:10.1029/2009JA015225.

Yashiro, S., N. Gopalswamy (2008), Statistical relationship between solar flares and coronal mass ejections, Universal Heliophysical Processes Proceedings IAU Symposium No. 257, 233–243, doi:10.1017/S1743921309029342.

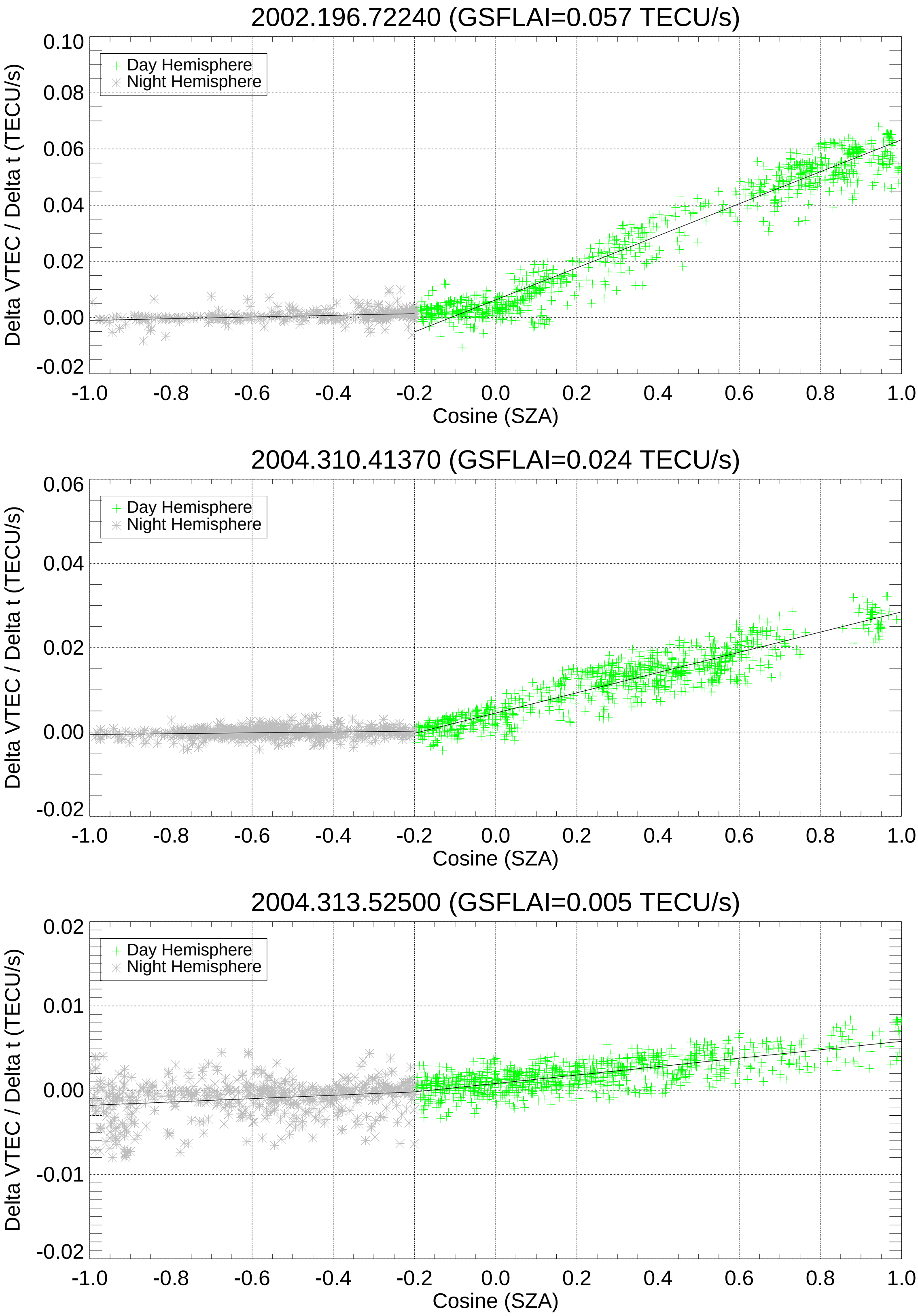

Figure 1. VTEC rate $\dot{V}$ vs $\cos \chi$ from top to bottom: a major X class Solar flare that occurred on day 196 of year 2002 at 72240 GPS time; an M class Solar flare that occurred on day 310 of year 2004; a C class flare on day 313 of year 2004 at 52500 GPS time. Data is fitted with a simple regression line individually for day and night hemispheres (note that the Y-axes are not at the same scale).

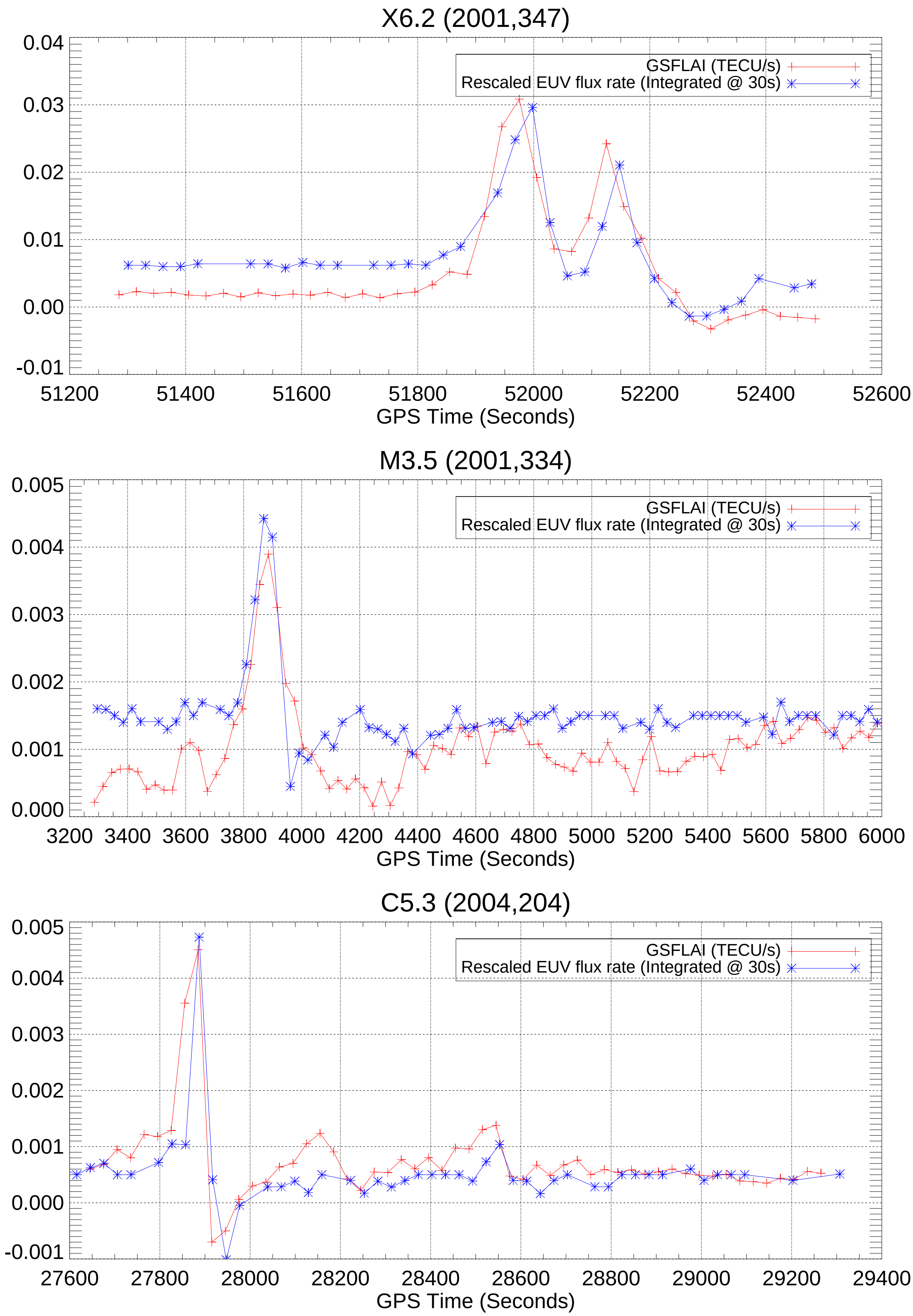

Figure 2. Correlation shown between GSFLAI and EUV flux rate data provided by SEM on-board SOHO for top to bottom: an X6.2 flare that occurred on day 347 of year 2001. EUV flux rate data is scaled as $\frac{0.165}{3{*}10^{10}} + 0.0046$; an M3.5 flare that occurred on day 334 of year 2001. EUV flux rate data is scaled as $\frac{0.157}{3{*}10^{10}} + 0.001$; a C5.3 flare that occurred on day 204 of year 2004. EUV flux rate data is scaled as $\frac{0.159}{3{*}10^{10}} + 0.0003$. (see also Table 1, columns 3 and 5)

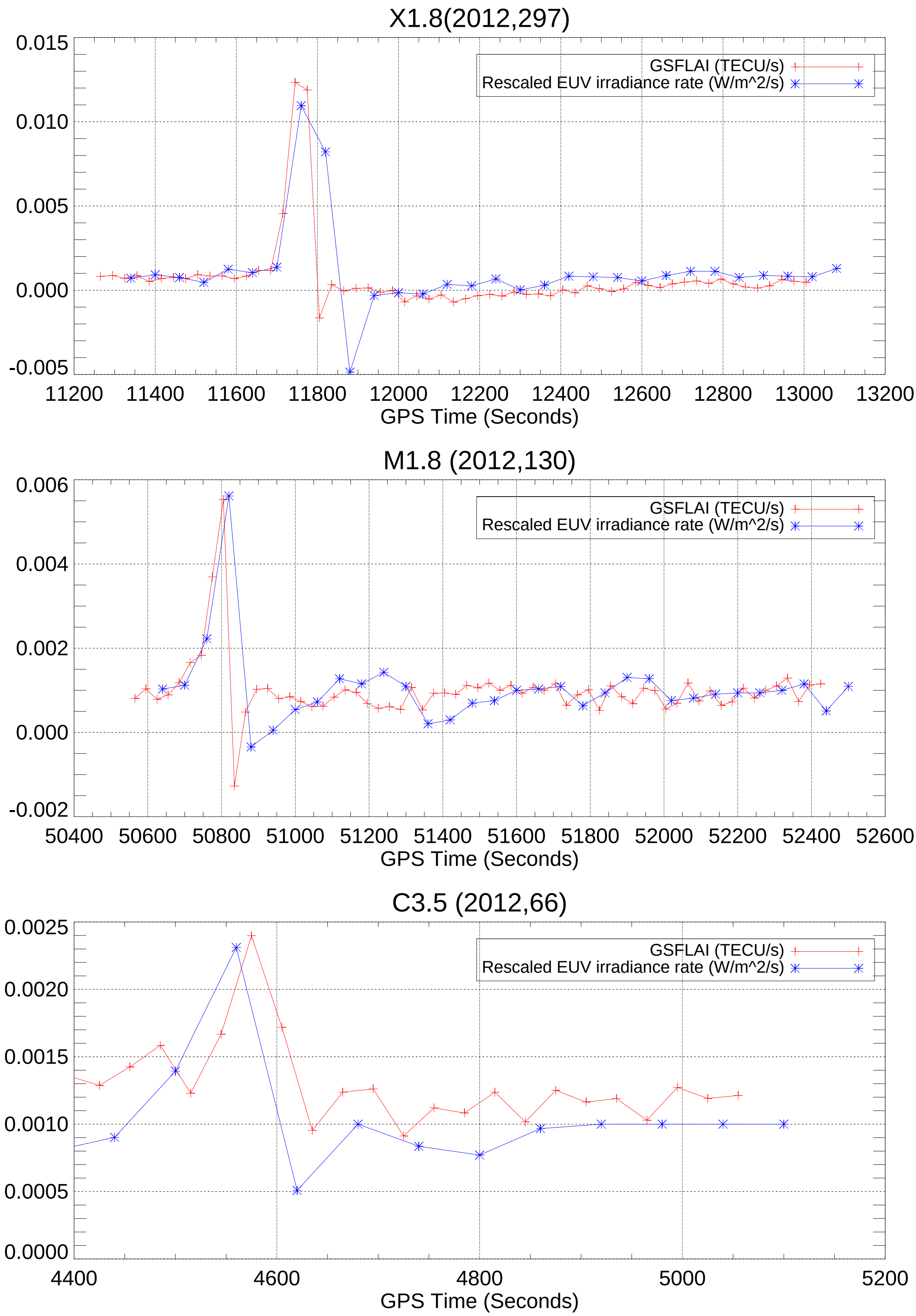

Figure 3. Correlation shown between GSFLAI and EUV irradiance rate data provided by channel B of EUVS on-board GOES-15 for top to bottom: an X1.8 flare that occurred on day 2977 of year 2012. EUV irradiance rate data is scaled as $2500.x + 0.001$; an M1.8 flare that occurred on day 130 of year 2012. EUV flux rate data is scaled as $1800.x + 0.001$; a C3.5 flare that occurred on day 66 of year 2012. EUV flux rate data is scaled as $2000.x + 0.001$.

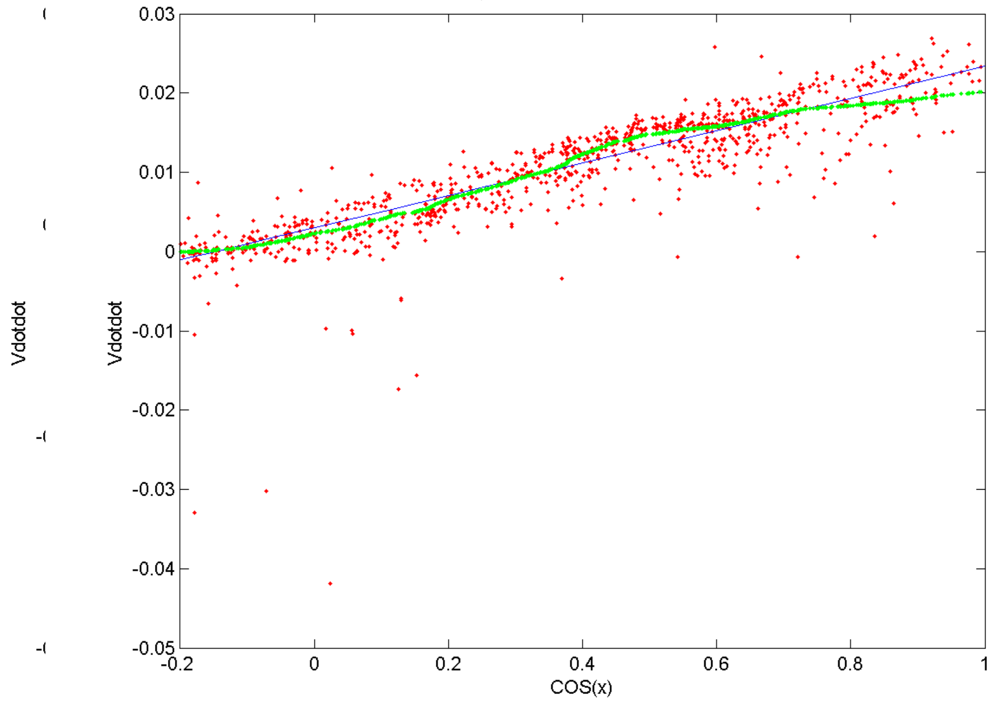

Figure 4. VTEC rate $\dot{V}$ vs $\cos\chi$ -red points-, compared with the regression line used in the study -blue line-, and the filtered VTEC rate -green points-, by means of a one dimensional median filter followed by a zero phase low pass filter: left, for a minor geoeffective Solar flare (GPS time 35970 seconds of day 310, 2013); right, for a mid geoeffective Solar flare (GPS time 30990 seconds of day 258, 2005)

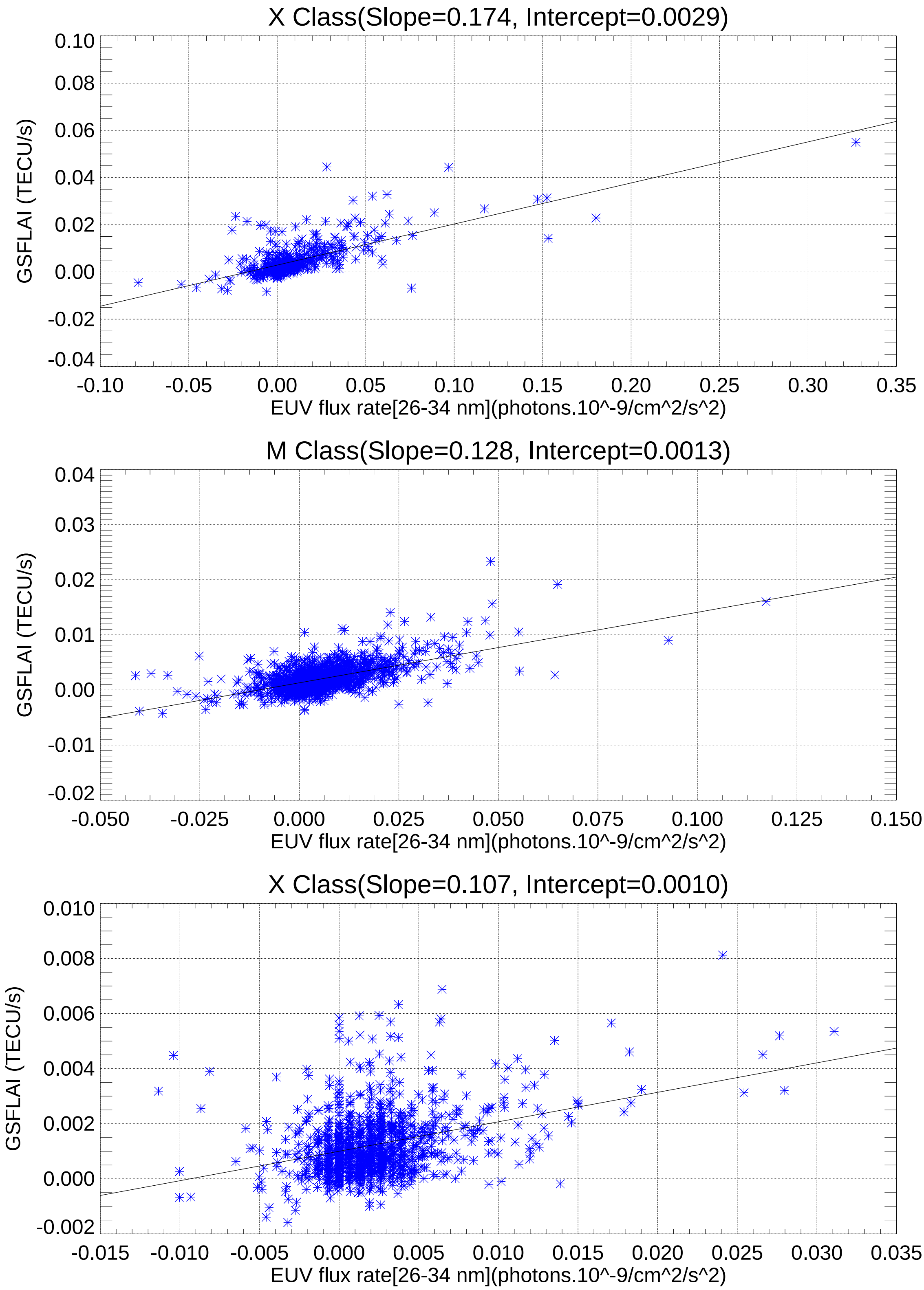

Figure 5. GSFLAI vs EUV flux rate data provided by SOHO-SEM in the 26-34 nm range for selected, top to bottom, X, M and C class flares which have occurred since 2001. Calculated simple regression lines are also shown for reference.

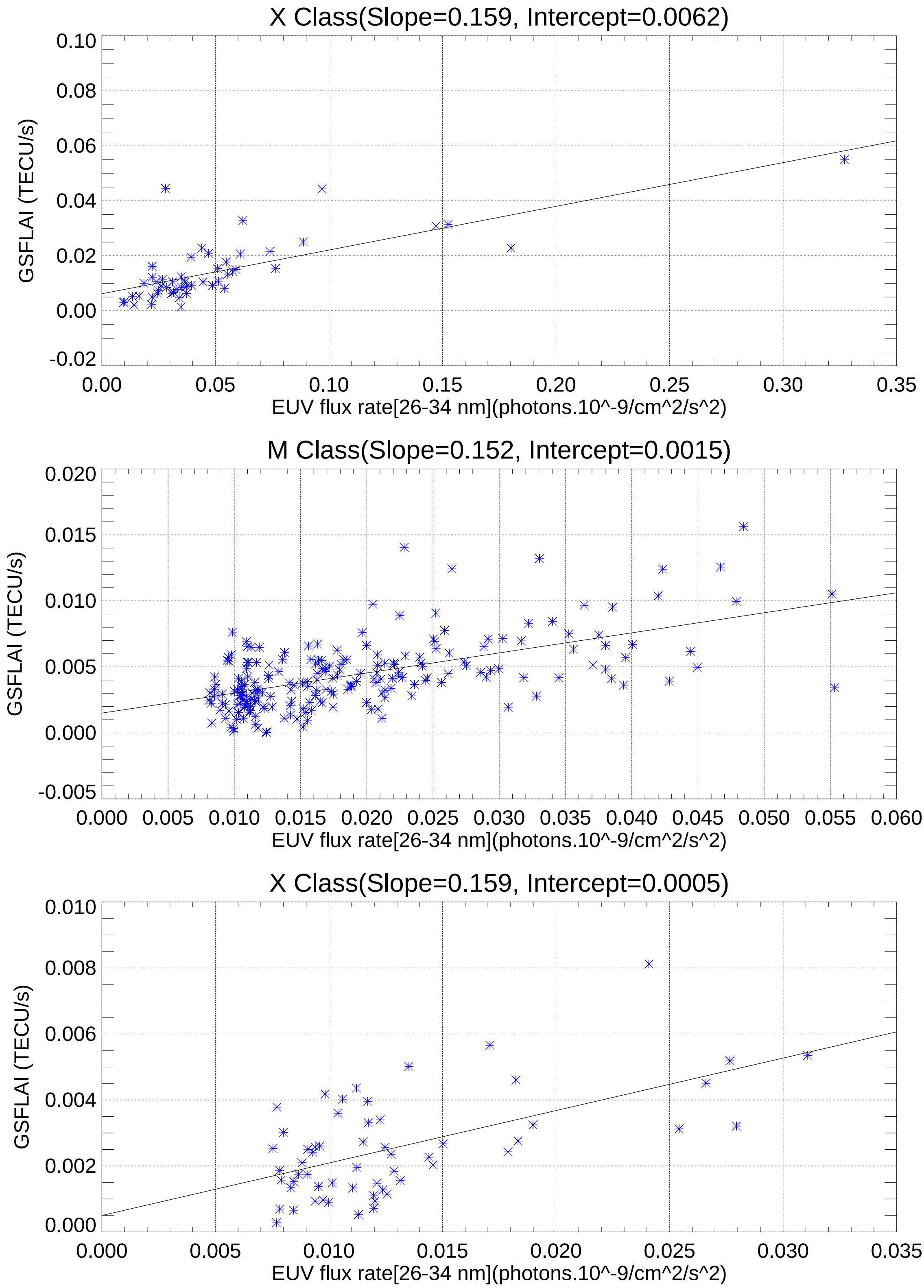

Figure 6. GSFLAI vs EUV flux rate data provided by SOHO-SEM in the 26-34 nm range for those points meeting specific criteria mentioned in Sec. 6.2 for top to bottom: X, M and C class flares which have occurred since 2001. Calculated simple regression lines are also shown for reference. Very few points are available for C class flares because EUV rate greater than 0.0075 $photons * 10^9/cm^2/s^2$ is rare in low intensity flares.

Table 1. Slope, intercept, correlation of linear fitting of GSFLAI (and corresponding P-values) vs SOHO/SEM Solar EUV flux rate (fifth seventh and ninth columns, respectively) and corresponding values when only GSFLAI peaks are taken (sixth, eighth and tenth columns), for X, M and C class flares (see the number of them in second column). [a]

Flares		No. of Points		Slope		Intercept		Corr. Factor		p values	
Class	Number	All	Peaks	All	Peaks	All	Peaks	All	Peaks		
X	59	523	53	0.174±0.008	0.159±0.006	0.0029±0.0002	0.0062±0.0015	0.69	0.73	0	0
M	323	1600	219	0.128±0.004	0.152±0.012	0.0013±0.00005	0.0015±0.0003	0.60	0.64	0	0
C	390	1163	58	0.107±0.008	0.159±0.029	0.0010±0.00004	0.0005±0.0004	0.35	0.59	0	$1.9 * 10^{-6}$

[a] The units are $TECU/s$ for GSFLAI and $photons.10^{-}9/cm^2/s^2$ for EUV flux rate.

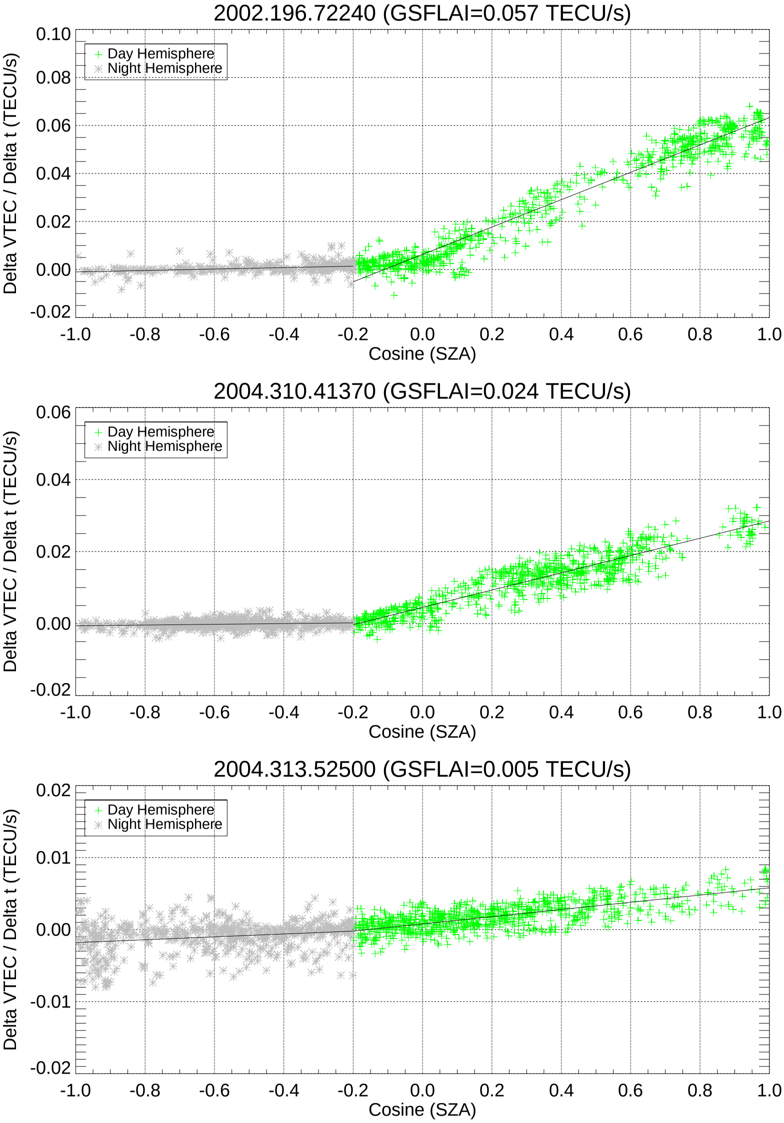

2002.196.72240 (GSFLAI=0.057 TECU/s)
Day Hemisphere
Night Hemisphere
Delta VTEC / Delta t (TECU/s)
0.10
0.08
0.06
0.04
0.02
0.00
-0.02
-1.0
-0.8
-0.6
-0.4
-0.2
0.0
0.2
0.4
0.6
0.8
1.0
Cosine (SZA)
2004.310.41370 (GSFLAI=0.024 TECU/s)
Day Hemisphere
Night Hemisphere
Delta VTEC / Delta t (TECU/s)
0.06
0.04
0.02
0.00
-0.02
-1.0
-0.8
-0.6
-0.4
-0.2
0.0
0.2
0.4
0.6
0.8
1.0
Cosine (SZA)
2004.313.52500 (GSFLAI=0.005 TECU/s)
Day Hemisphere
Night Hemisphere
Delta VTEC / Delta t (TECU/s)
0.02
0.01
0.00
-0.01
-0.02
-1.0
-0.8
-0.6
-0.4
-0.2
0.0
0.2
0.4
0.6
0.8
1.0
Cosine (SZA)

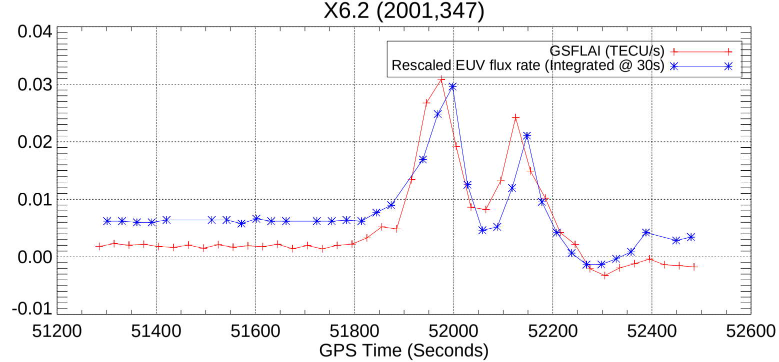
X6.2 (2001,347)
GSFLAI (TECU/s)
Rescaled EUV flux rate (Integrated @ 30s)
GPS Time (Seconds)

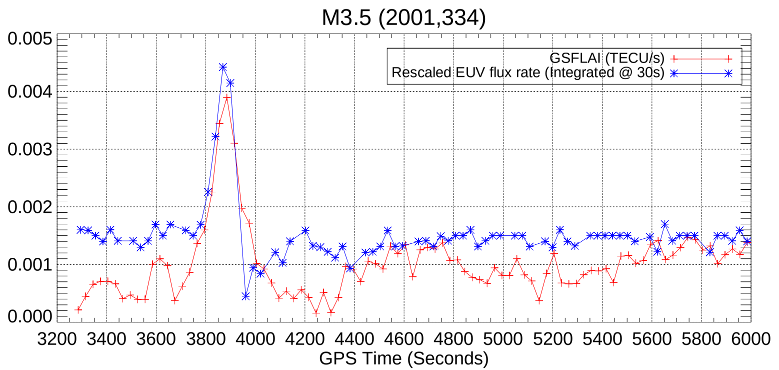
M3.5 (2001,334)
GSFLAI (TECU/s)
Rescaled EUV flux rate (Integrated @ 30s)
GPS Time (Seconds)

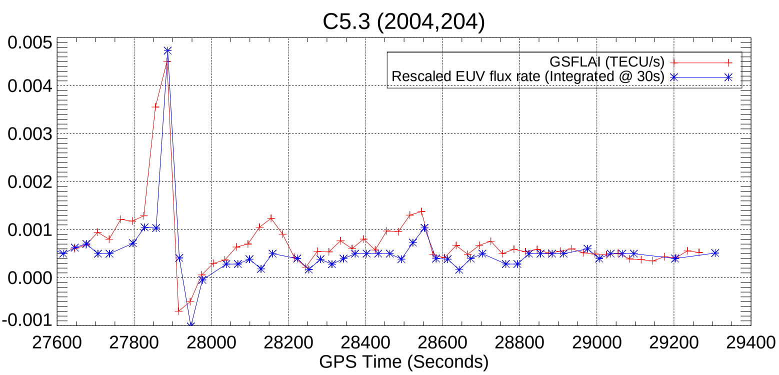
C5.3 (2004,204)
GSFLAI (TECU/s)
Rescaled EUV flux rate (Integrated @ 30s)
GPS Time (Seconds)

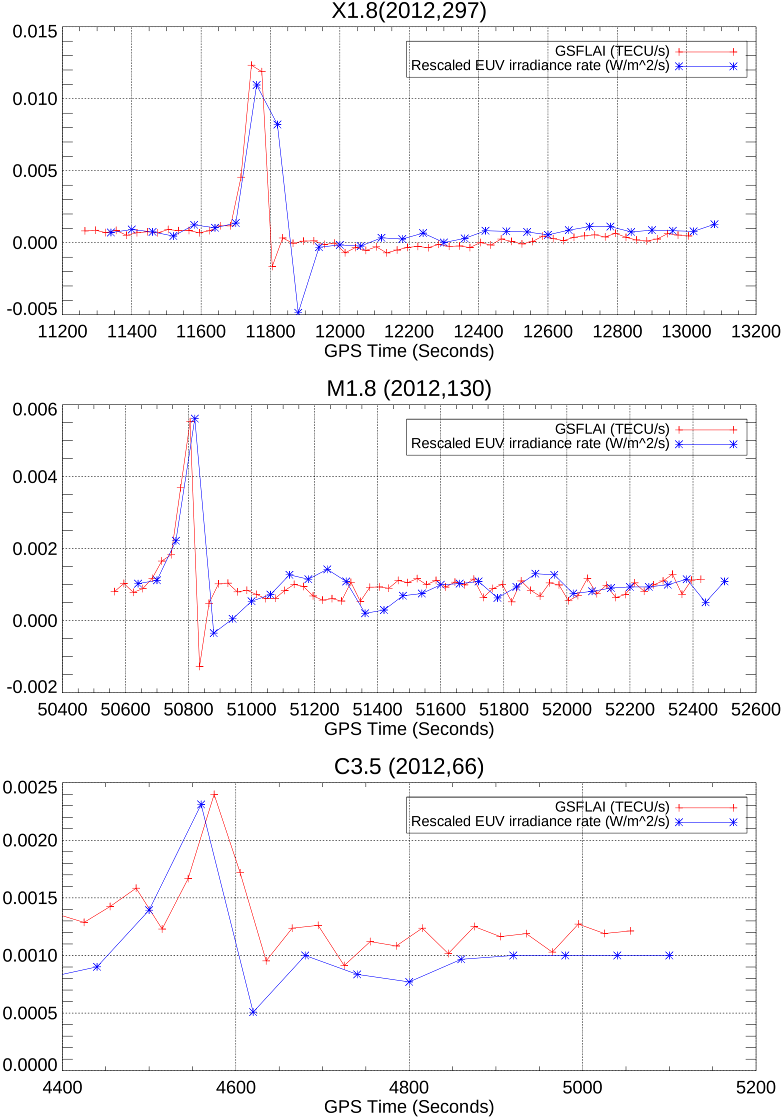
X1.8(2012,297)
GSFLAI (TECU/s)
Rescaled EUV irradiance rate (W/m^2/s)
GPS Time (Seconds)
M1.8 (2012,130)
GSFLAI (TECU/s)
Rescaled EUV irradiance rate (W/m^2/s)
GPS Time (Seconds)
C3.5 (2012,66)
GSFLAI (TECU/s)
Rescaled EUV irradiance rate (W/m^2/s)
GPS Time (Seconds)

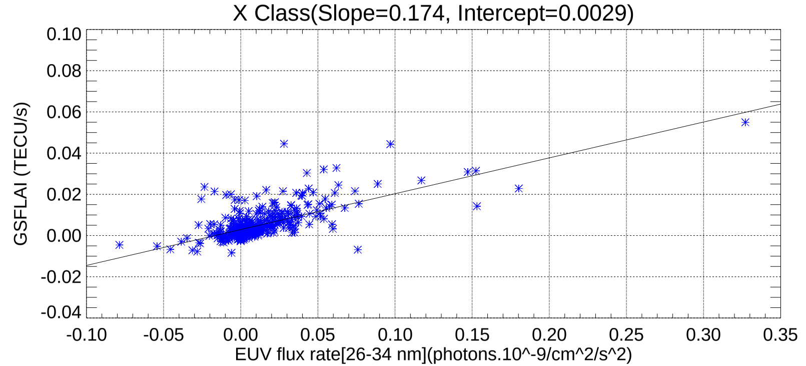
X Class(Slope=0.174, Intercept=0.0029)
GSFLAI (TECU/s)
EUV flux rate[26-34 nm](photons.10^-9/cm^2/s^2)

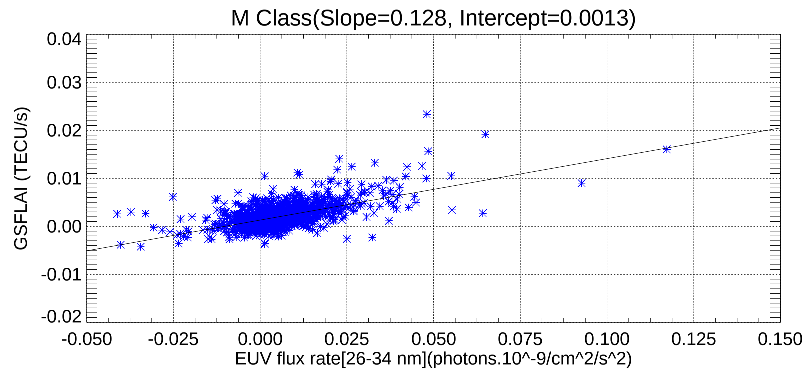
M Class(Slope=0.128, Intercept=0.0013)
GSFLAI (TECU/s)
EUV flux rate[26-34 nm](photons.10^-9/cm^2/s^2)

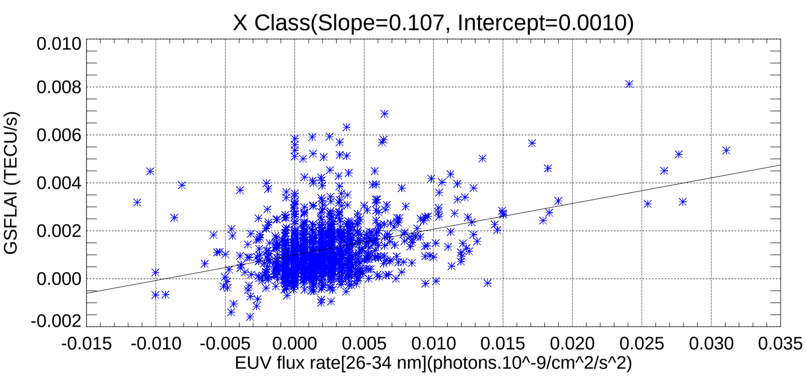
X Class(Slope=0.107, Intercept=0.0010)
GSFLAI (TECU/s)
EUV flux rate[26-34 nm](photons.10^-9/cm^2/s^2)

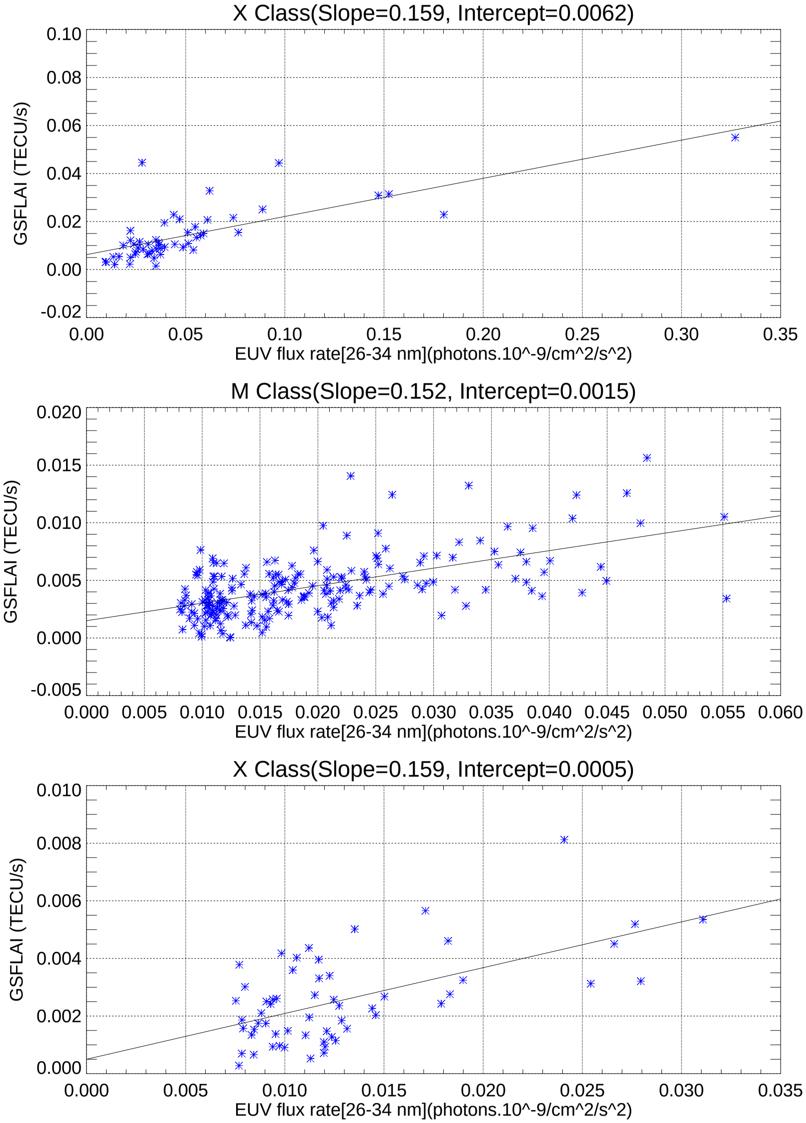

X Class(Slope=0.159, Intercept=0.0062)
GSFLAI (TECU/s)
EUV flux rate[26-34 nm](photons.10^-9/cm^2/s^2)
M Class(Slope=0.152, Intercept=0.0015)
GSFLAI (TECU/s)
EUV flux rate[26-34 nm](photons.10^-9/cm^2/s^2)
X Class(Slope=0.159, Intercept=0.0005)
GSFLAI (TECU/s)
EUV flux rate[26-34 nm](photons.10^-9/cm^2/s^2)

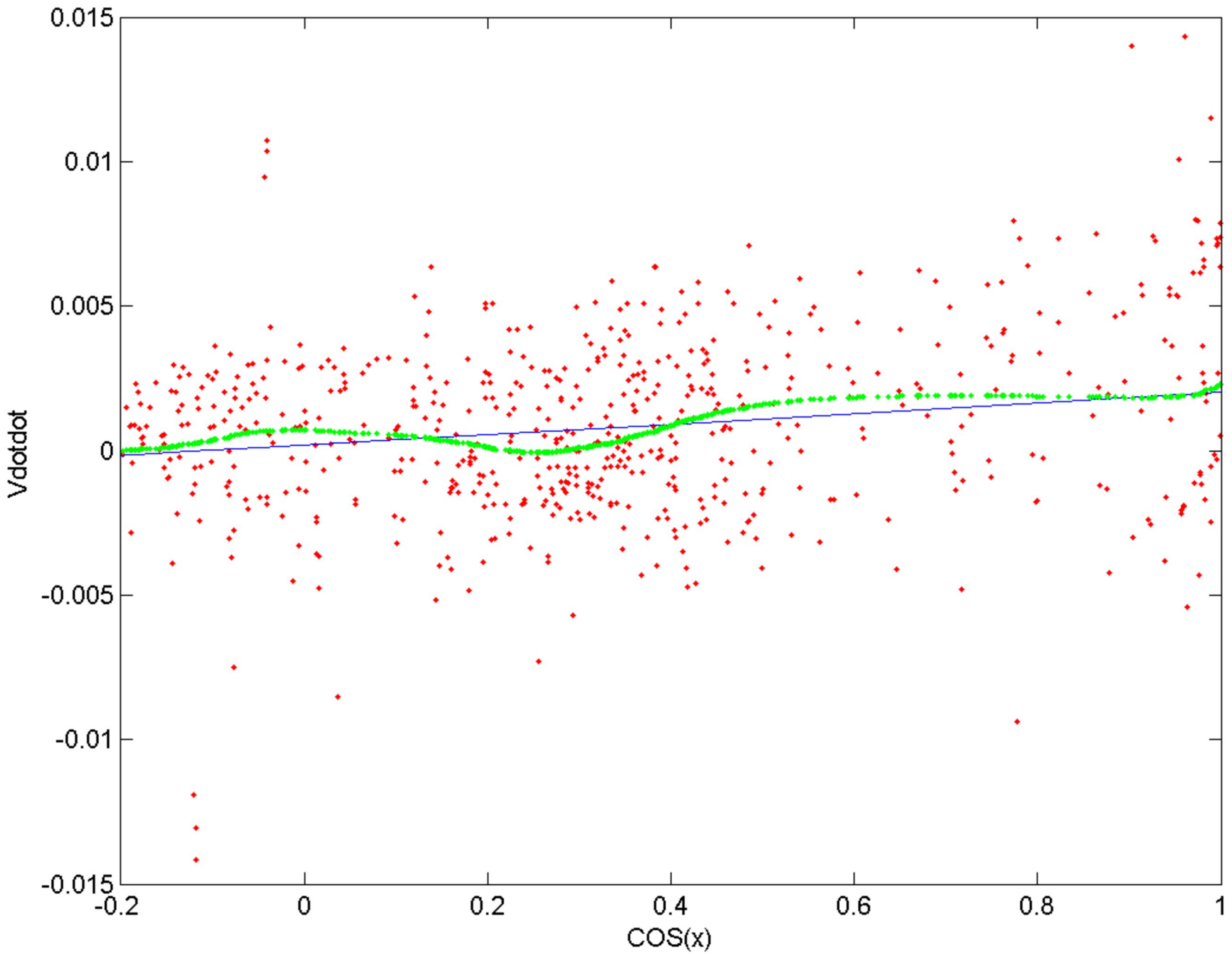

0.015
0.01
0.005
0
-0.005
-0.01
-0.015
-0.2
0
0.2
0.4
0.6
0.8
1
Vdotdot
COS(x)

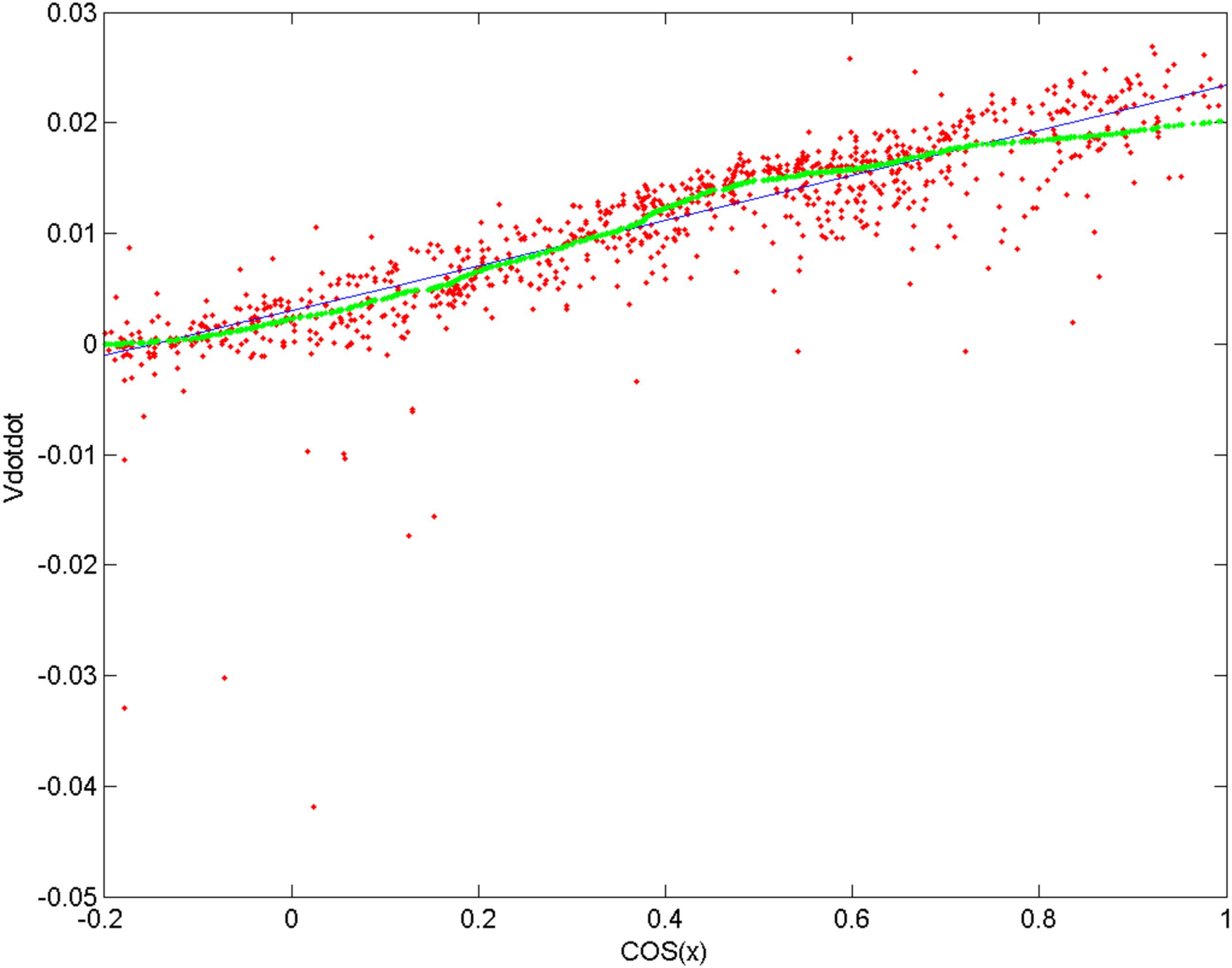
0.03
0.02
0.01
0
-0.01
-0.02
-0.03
-0.04
-0.05
Vdotdot
-0.2
0
0.2
0.4
0.6
0.8
1
COS(x)